JOURNAL OF MATERIALS SCIENCE 30 (1995) 5681–5686

The orientation relationship between tetragonal zirconia precipitates with regard to elastic interaction energy

D. G. JENSEN
Department of Materials Engineering, Monash University, Wellington Road, Clayton, Victoria 3168, Australia

The elastic interaction energy between tetragonal zirconia precipitates for different mutual orientations is considered. The results of numerical analysis of this procedure are compared with experimentally observed preferred orientation relationships in the ceria–magnesia-partially stabilized zirconia (CM–PSZ) system. Two variants appear favourable, a parallel-stepped precipitate configuration with precipitate centres stepped at about 20°, and orthogonal precipitates in an edge-face configuration.

1. Introduction

The orientation of precipitates with regard to one another is primarily dependent on the minimization of their interaction energy [1]. Perovic *et al.* [2] found precipitates tended to align preferentially either orthogonally or parallel in a rafted manner; in detail, however, calculations showed that interaction energy between parallel precipitates should occur when the precipitates are coplanar. This does not occur in practice, and Bhathena *et al.* [3] attempted to explain this by means of autocatalytic nucleation resulting from the solute gradient surrounding the precipitate. It is our belief that the rafted microstructure is a result of the more fundamental interaction energy, and we have embarked on a numerical analysis procedure in order to explain this rafting, as well as attempting to explain some of the other orientation relationships observed experimentally in partially stabilized zirconia systems.

Transformation-toughened partially stabilized zirconias take advantage of the transformation of precipitates from the tetragonal to the monoclinic phase as a toughening mechanism. This transformation is a result of a partial relaxation of the constraint imposed by the cubic matrix; this is often associated with the nearby propagation of a crack [4]. The transformation from tetragonal to monoclinic is accompanied by a 4% volume increase, and it is this associated volume expansion that absorbs some of the energy normally used to continue the crack's propagation. The effectiveness of this toughening mechanism, however, is limited to temperatures below about 300 °C; above this temperature, the thermodynamics of the system are such that the tetragonal phase becomes more stable, reducing the propensity for the precipitates to undergo a stress-induced transformation to monoclinic.

In order to surmount this problem, other potential toughening mechanisms such as crack bridging, crack deflection, and microcrack toughening, need to be invoked [5, 6]. To this end we have embarked on a program to develop a system with a microstructure that maximizes the potential toughening increment utilizing these other mechanisms.

These other mechanisms depend not only on phase content, but also on the microstructure of the precipitates, and their mutual orientation relationships. In order to understand better the observed microstructure, and to determine the potential for developing and controlling microstructures of different orientation relationships, elastic interaction energies have been calculated to ascertain which of the orientation relationships are potentially energetically favorable.

2. Experimental procedure

Material of composition 1.25 mol % CeO_2, 10.8 mol % MgO and ZrO_2 were attritted, spray dried, pressed into pellets and fired at 1700 °C for 5 h. The pellets were subsequently aged for different periods of time at 1400 °C. TEM samples, 3 mm in size, were prepared by dimple grinding, then ion-beam thinning to perforation, and application of a light carbon coat.

TEM analysis was undertaken using a Philips EM420 microscope operated at 120 kV. Imaging conditions were set up close to the $\langle 1\,0\,0 \rangle$ direction (precipitates in this system lie along $\langle 1\,0\,0 \rangle$ type cubic lattice directions).

3. Estimation of elastic interaction energy between tetragonal precipitates

It is desired to calculate the interaction energy of two equally sized precipitates of distance R apart (where $R = (c^2 + h^2)^{1/2}$, see Figs 1 and 3).

0022–2461

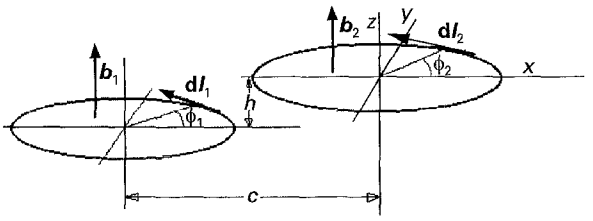

Figure 1 Schematic representation for the case of orthogonal precipitates. Here c is parallel to the x-axis and h is parallel to the y-axis.

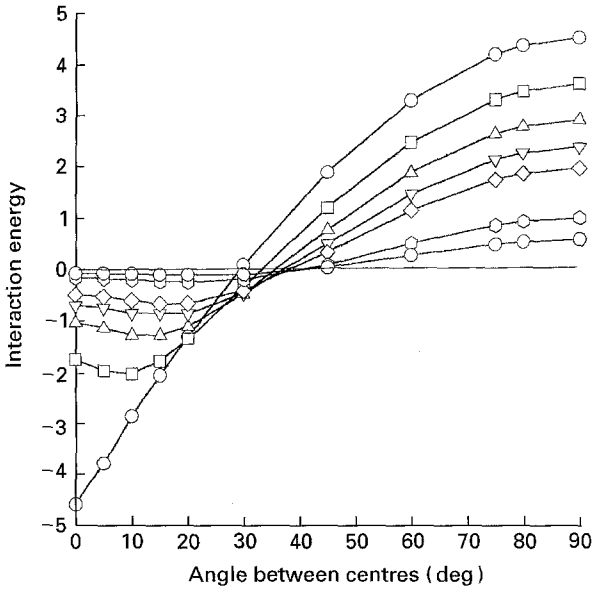

Figure 2 Standardized interaction energy versus θ for parallel precipitates. θ = 0° represents the coplanar case, θ = 90° is the coaxial case. R = (○) $2a$, (□) $2.25a$, (△) $2.5a$, (▽) $2.75a$, (◇) $3a$, (○) $4a$, (○) $5a$.

To enable reasonable ease of calculation of interaction energies, two assumptions are made. First, it is assumed that all of the strain is normal to the habit plane of the precipitate; this is not unreasonable; for the system under investigation this strain is about two orders of magnitude greater than the strain parallel to the precipitate [7]. Second, the medium is considered to be elastically isotropic; once again, this is not an unreasonable assumption, as zirconia is known to be one of the more elastically isotropic materials.

For the purposes of this analysis, precipitates are taken to be discs of radius a (they are, in fact, ellipsoids) with a Burgers vector of magnitude εt, where ε is the strain and t is the thickness of the precipitate [8, 9].

3.1. Example of the calculation of interaction strain energy between orthogonal precipitates

The interaction energy between two precipitates is [10]

$$E_{12} = \int dA_{1\beta} b_{1\alpha} \sigma_{2\alpha\beta} \tag{1}$$

or, in expanded form

$$E_{12} = -\frac{\mu}{2\pi}\oint\oint\frac{(\boldsymbol{b}_1 x \boldsymbol{b}_2)(\mathbf{d}\boldsymbol{l}_1 x \mathbf{d}\boldsymbol{l}_2)}{R} + \frac{\mu}{4\pi}\oint\oint\frac{(\boldsymbol{b}_1 \mathbf{d}\boldsymbol{l}_1)(\boldsymbol{b}_2 \mathbf{d}\boldsymbol{l}_2)}{R} + \frac{\mu}{4\pi(1-\nu)}\oint\oint(\boldsymbol{b}_1 x \mathbf{d}\boldsymbol{l}_1)\boldsymbol{T}(\boldsymbol{b}_2 x \mathbf{d}\boldsymbol{l}_2) \tag{2}$$

where

$$\boldsymbol{T}_{ij} = \frac{\partial^2 R}{\partial x_i \partial x_j} \tag{3}$$

$$R = (x^2 + y^2 + z^2)^{1/2} \tag{4}$$

where

$$x = c - a\cos(\phi) \tag{5}$$

$$y = a[\sin(\theta) - \sin(\phi)] + h \tag{6}$$

$$z = a\cos(\theta) \tag{7}$$

$$\frac{\partial^2 R}{\partial x^2} = \frac{y^2 + z^2}{R^3} \tag{8}$$

$$\frac{\partial^2 R}{\partial y^2} = \frac{x^2 + y^2}{R^3} \tag{9}$$

$$\frac{\partial^2 R}{\partial z^2} = \frac{x^2 + y^2}{R^3} \tag{10}$$

$$\frac{\partial^2 R}{\partial x \partial y} = \frac{-xy}{R^3} \tag{11}$$

$$\frac{\partial^2 R}{\partial x \partial z} = \frac{-xz}{R^3} \tag{12}$$

$$\frac{\partial^2 R}{\partial y \partial z} = \frac{-yz}{R^3} \tag{13}$$

and

$$\boldsymbol{b}_1 = (0, 0, b) \tag{14}$$

$$\boldsymbol{b}_2 = (b, 0, 0) \tag{15}$$

$$\mathbf{d}\boldsymbol{l}_1 = [-\sin(\phi), \cos(\phi), 0]\,ad(\phi) \tag{16}$$

$$\mathbf{d}\boldsymbol{l}_2 = [0, -\cos(\theta), \sin(\theta)]\,ad(\theta) \tag{17}$$

so

$$(\boldsymbol{b}_1 x \mathbf{d}\boldsymbol{l}_1) = bad(\phi)[-\cos(\phi), -\sin(\phi), 0] \tag{18}$$

$$(\boldsymbol{b}_2 x \mathbf{d}\boldsymbol{l}_2) = bad(\theta)[0, -\sin(\theta), -\cos(\theta)] \tag{19}$$

$$(\boldsymbol{b}_1 x \boldsymbol{b}_2) = (0, b^2, 0) \tag{20}$$

$$(\mathbf{d}\boldsymbol{l}_1 x \mathbf{d}\boldsymbol{l}_2) = a^2 d(\phi) d(\theta)[\cos(\phi)\sin(\theta), \sin(\phi)\sin(\theta), \sin(\phi)\cos(\theta)] \tag{21}$$

For our case, where the Burger's vector and the line element on the circumference of the disc are orthogonal, the first term in the integrand is

$$(\boldsymbol{b}_1 x \boldsymbol{b}_2)(\mathbf{d}\boldsymbol{l}_2 x \mathbf{d}\boldsymbol{l}_2) = b^2 a^2 \sin(\phi)\sin(\theta) d(\phi) d(\theta) \tag{22}$$

The second term in the integrand = 0.

The third term in the integrand is given by

$$(\boldsymbol{b}_1 x \mathrm{d}\boldsymbol{l}_1)\, T(\boldsymbol{b}_2 x \mathrm{d}\boldsymbol{l}_2)$$

$$\rightarrow \frac{b^2a^2\mathrm{d}(\phi)d(\theta)}{R^3}[-\cos(\phi), -\sin(\phi), 0] \otimes$$

$$\begin{bmatrix} (y^2+z^2) & (-xy) & (-xz) \\ (-xy) & (x^2+z^2) & (-yz) \\ (-xz) & (-yz) & (x^2+y^2) \end{bmatrix} \otimes \begin{bmatrix} 0 \\ -\sin(\theta) \\ -\cos(\theta) \end{bmatrix}$$

$$= \frac{b^2a^2\mathrm{d}(\phi)d(\theta)}{R^3}[\cos(\phi)[-xy\sin(\theta) - xz\cos(\theta)]$$

$$+ \sin(\phi)[(x^2+z^2)\sin(\theta) - yz\cos(\theta))] \quad (23)$$

This gives the terms for the interaction energy

$$E_{12} = \frac{-\mu a^2b^2}{2\pi}\int\int\frac{\sin(\phi)\sin(\theta)\mathrm{d}(\phi)\mathrm{d}(\theta)}{R}$$

$$+\frac{\mu a^2b^2}{4\pi(1-\nu)}\int\int(\{\cos(\phi)(-xy\sin(\theta) - xz\cos(\theta))$$

$$+ \sin(\phi)[(x^2+z^2)\sin(\theta) - yz\cos(\theta)]\}\mathrm{d}(\phi)\mathrm{d}(\theta))/R^3 \quad (24)$$

Substitution for x, y and z (given previously), and also substitutions for c and a will allow numerical integration to be carried out. ν was taken to be 0.33. Additionally, if V is taken as $\pi a^2 b$, the interaction energy can be calculated for discs having a volume V.

3.2. Parallel, but not necessarily coplanar, precipitates

Here, the functions have the following form

$$x = c + a[\cos(\phi_2) - \cos(\phi_1)] + c \quad (25)$$

$$y = a[\sin(\phi_2) - \sin(\phi_1)] \quad (26)$$

$$z = h \quad (27)$$

$$(\boldsymbol{b}_1 x \boldsymbol{b}_2)(\mathrm{d}\boldsymbol{l}_1 x \mathrm{d}\boldsymbol{l}_2) = 0 \quad (28)$$

so only the third term in the integrand applies.

In similar manner to that for the calculation of orthogonal precipitates, the interaction energy for the system is obtained

$$E_{12} = \frac{\mu a^2b^2}{4\pi(1-\nu)}\int\int(\{\cos(\phi_1)[\cos(\phi_2)(y^2+z^2)$$

$$- xy\sin(\phi_2)] + \sin(\phi_1)[-xy\cos(\phi_2)$$

$$+ (x^2+z^2)\sin(\phi_2)]\}\mathrm{d}(\phi_1)\mathrm{d}(\phi_2))/R^3 \quad (29)$$

4. Numerical evaluation

Our evaluation of interaction strain energies between two precipitates (discs) was carried out for different values of R; the numerical integration involved holding this distance constant while moving one of the precipitates through an arc of 90° with regard to the other. Once the calculations had been carried out for one value of R, the process was repeated for the next value. Proceeding in this manner allowed the investigation of the relative effects of both inter-precipitate distance variation and the variation of precipitate orientation relationships. This will be discussed in more detail later.

4.1. Parallel precipitates

The precipitate orientation was moved from $\theta = 0°$, which is the coplanar orientation (edge–edge) to $\theta = 90°$, which is the coaxial orientation (face–face) (see Fig. 1); the results of the elastic strain interaction energy are given in Fig. 2.

It is found that if the centre–centre distance is any less than $2R$, the interaction energy is positive for all angles. As the precipitate centres become separated by $2a$ (i.e. in the coplanar case they are touching), it is found that the interaction energy becomes strongly negative, and that for this distance between their respective centres, the energy minima coincides with the coplanar situation.

As the precipitates are moved further apart, it is found that the position of the energy minima with regard to the respective centres shifts from a coplanar position at $2a$ to $\theta = 20°$ when the centre–centre distance $\geqslant 2.75a$. (This is probably due to the positive interaction when any part of the precipitates overlap; this overlapping portion has strong positive interaction energy due to the face–face configuration). Although Perovic *et al.* [1, 2, 11] obtain an energy minimum that coincides for coplanar precipitates at all separations, it is found not to be the case here. This may be due to Perovic *et al.* moving the precipitates parallel to one of the axes; this would have the effect of increasing or decreasing the centre–centre distance. In all probability, the actual variation in interaction energy is clouded by the variation in centre–centre distance between the precipitates as calculated by Perovic *et al.* Clearly, moving a precipitate along the z-axis will increase the inter-particle spacing, giving rise to a smaller magnitude of interaction energy, which would tend to indicate an energy minimum for the coplanar case.

Bhathena *et al.* [3] invoke the existence of a solute gradient in order to explain the rafting of precipitates in a non-coplanar fashion; although the leaching of the stabilizer from the precipitate to the surrounding matrix is certainly a contributing factor for the distance from the pre-existing precipitate of possible nucleation sites, in our view it is not the dominant one. This solute gradient stabilizes the cubic matrix phase in close proximity to the precipitate, requiring that another precipitate would have to nucleate some distance from the pre-existing precipitate; it does not, however, give any idea of a favourable orientation. The nucleation site is decided by the minimization (or local minimization) of the interaction strain energy, with due regard to the local solute concentration. For parallel precipitates, this requires that one precipitate, in exclusion of interactions of all other precipitates bar the one in question, will nucleate at about 20° to the precipitate plane.

4.2. Orthogonal variants

Precipitates may be orthogonal to each other in either a face–edge or edge–edge orientation. In order to do a complete evaluation of the effects of the orientation and distance between two orthogonal precipitates, we proceeded in the same manner as for the parallel

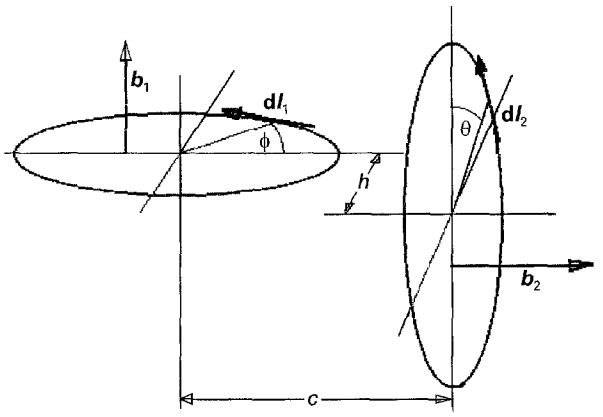

Figure 3 Schematic representation for the case of parallel precipitates. Angles are given by $c = R\,\mathrm{Cos}\,\theta$, $h = R\sin\theta$ where c is parallel to the x-axis and h is parallel to the z-axis.

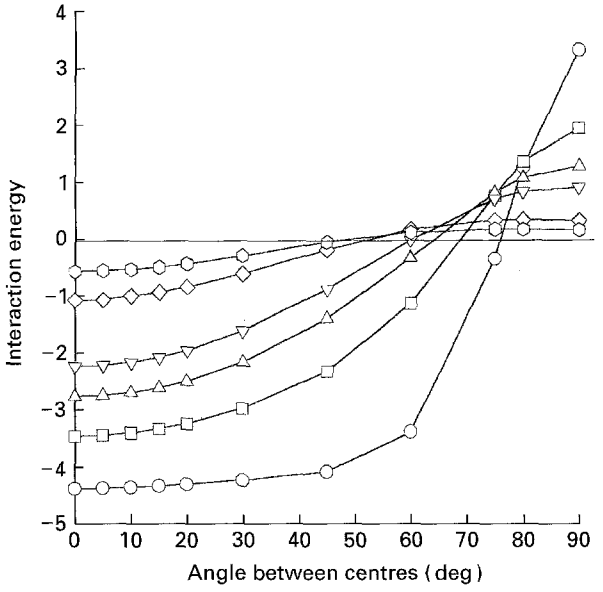

Figure 4 Standardized interaction energy versus θ for orthogonal precipitates. $\theta = 0°$ represents the edge–face orientation, $\theta = 90°$ represents the edge–edge orientation. R = (○) 2.25a, (□) 2.5a, (△) 2.75a, (▽) 3a, (◇) 4a, (○) 5a.

variants, from $\theta = 0°$ representing the edge–face orthogonal variants, to $\theta = 90°$ representing the edge–edge orthogonal orientation (see Fig. 3). The results of the numerical analysis for this orientation are given in Fig. 4.

From Fig. 4, it is clear that when the precipitate centres are close together, the interaction energy minimum is fairly broad, or degenerates, with regard to orientation away from the face–edge orientation (within approximately 50°). When further apart, the minimum is not so broad, and for $R = 5a$, the interaction energy graph passes through zero at about 45° from the edge–face position, whereas for $R = 2.25a$, this angle is about 75°.

In all probability, this is due to precipitates in close proximity having one part of the precipitate in very close edge–face proximity to the other, which would give a very large negative interaction energy; this would more than compensate for the reduced negative interaction energy further away from the "edge–face" configuration (as is indicated where $R = 5a$). From a nucleation point of view, therefore, the precipitate will nucleate off the edge (i.e. 0°) of the pre-existing precipitate, at a distance where the local solute concentration allows this to occur.

Interestingly, the edge–edge orthogonal relationship is strongly repulsive (about half the face–face positive interaction energy), which would make this configuration energetically unfavourable, unless this occurred in the vicinity of another precipitate in the edge–face position. A nearby precipitate in the edge–face position would allow two other precipitates to have an edge–edge orientation to each other, provided the net interaction energy was negative.

5. Discussion

The data indicate that the most energetically favourable configuration is the edge–face orthogonal case. The edge–edge parallel case, while still energetically favourable, would be expected to occur less frequently than the edge–face orthogonal configuration due to the smaller magnitude of the interaction energy. Experimentally, this is found to be the case, with parallel configurations only evident in the case of rafting of more than two precipitates, usually at an angle of about 20° (see Fig. 5); a coplanar orientation is never evident.

By far the predominant configuration observed is that of the edge–face orthogonal variants; the interaction energy for this case is very strong, and with large precipitates is assumed to be related to the observed faceting, as is evinced by alignment of the facet apex with the orthogonal variant [12] (see Fig. 6).

Occasionally, precipitates are found in the face–face energetically unfavourable orientation. It is difficult to determine if this occurs where there are unseen (by TEM) edge–face orthogonal precipitates to the face–face precipitates, where the net contribution would be energetically favourable (see Fig. 7). What is clear here, however, is that there is strong strain-induced diffraction contrast in the matrix, giving a qualitative idea of the strong positive interaction energy between these precipitates. Orthogonal variants in the edge–face orthogonal configuration do not generally show this strain contrast, despite having a larger net interaction energy; this is because the precipitates themselves appear to accommodate the strain interaction.

With regard to Fig. 7, two further items of interest are indicated in the micrograph; these are labelled (a) and (b). The long precipitate observed in (a) can be seen to have many breaks along its length, probably due to the joining together of a raft of precipitates. Precipitate (b) appears to be the result of an intergrowth of two precipitates; the intergrowth area between the two precipitates is probably a result of a local solute deficiency.

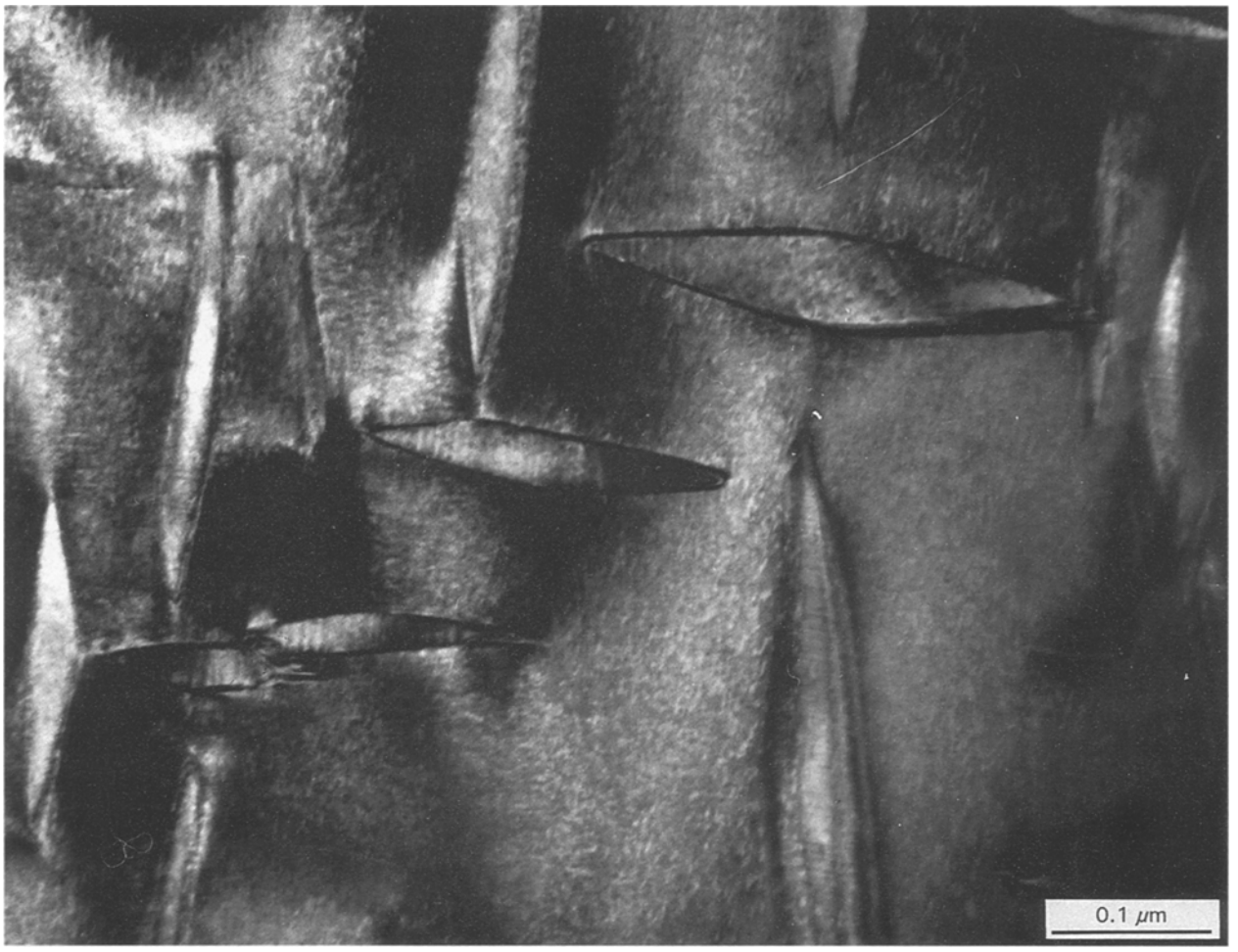

Figure 5 Transmission electron micrograph of tetragonal precipitates in CM–PSZ, showing the rafting common for parallel variants.

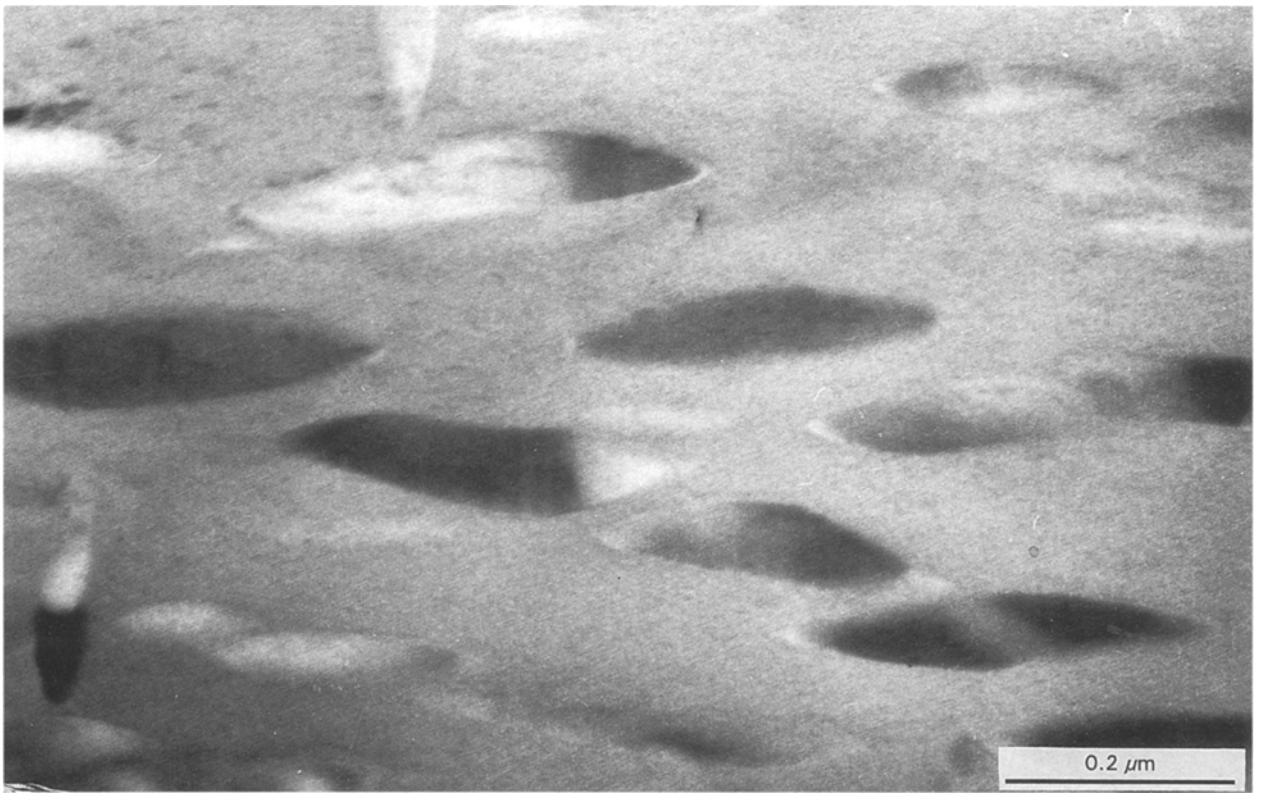

Figure 6 Transmission electron micrograph of orthogonal edge–face precipitates. Note the accommodation of strain in the precipitates themselves, manifested as faceting on the face of the precipitate facing its orthogonal partner's edge.

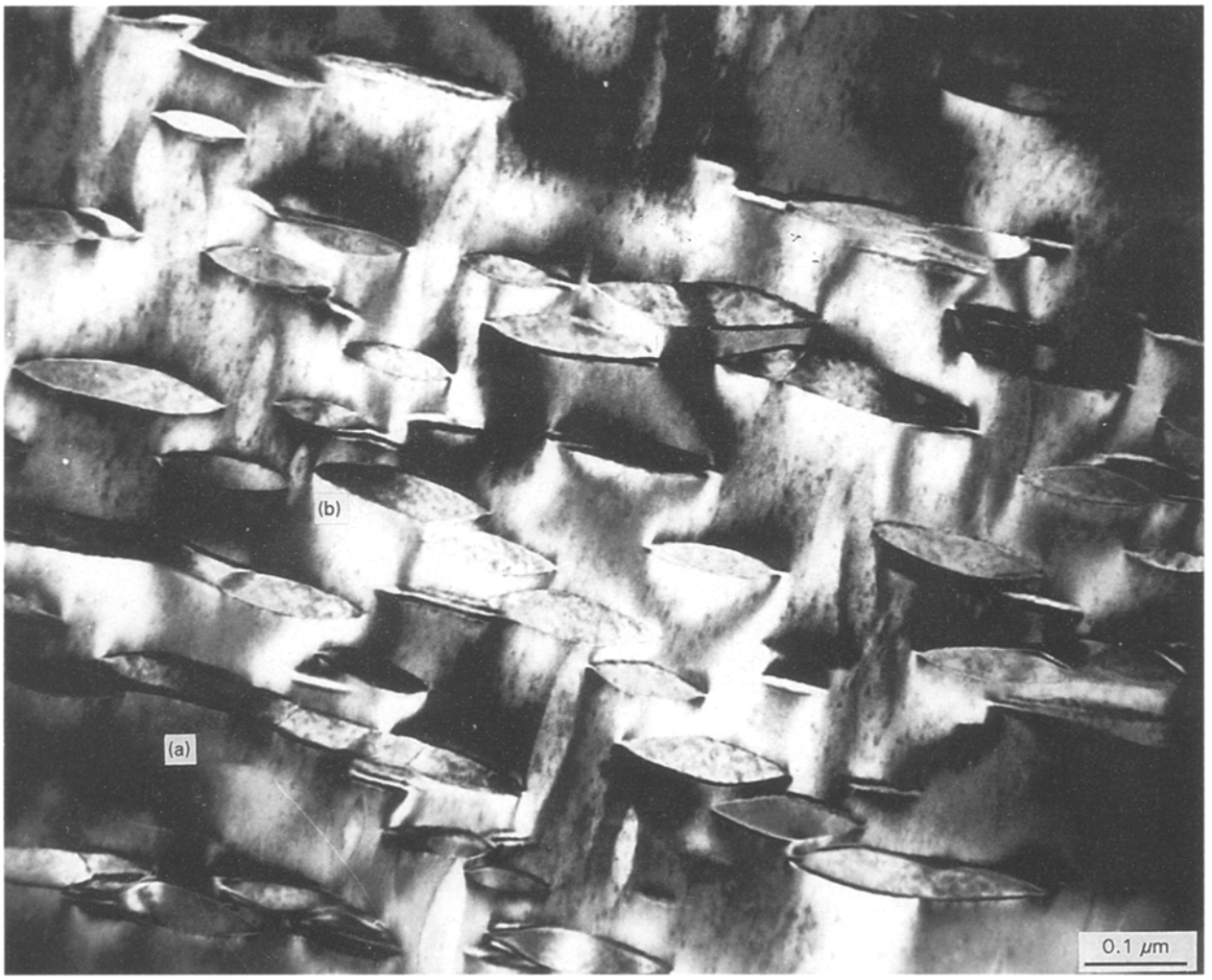

Figure 7 Parallel precipitates in the face–face configuration. There may be unseen precipitates in the plane of the micrograph which would reduce the net interaction energy. Note the strong strain contrast in the matrix. Regions marked (a) and (b) are discussed in the text.

Acknowledgement

The author gratefully acknowledges the help provided by V. W. Maslen in setting up the integral equations.

References

1. V. PEROVIC, G. R. PURDY and L. M. BROWN, *Acta Metall.* **27** (1979) 1075.
2. *Idem, ibid.* **29** (1981) 889.
3. N. BHATHENA, R. G. HOAGLAND and G. MEYRICK, *J. Am. Ceram. Soc.* **67** (1984) 799.
4. D. J. GREEN, R. H. J. HANNINK and M. V. SWAIN, "Transformation toughening of ceramics" (CRC Press, 1989).
5. A. G. EVANS, *J. Am. Ceram. Soc.* **73** (1990) 187.
6. R. W. STEINBRECH, *J. Eur. Ceram. Soc.* **10** (1992) 131.
7. D. G. JENSEN, R. H. J. HANNINK and B. C. MUDDLE, unpublished results.
8. V. LANTERI, T. E. MITCHELL and A. H. HEUER, *J. Am. Ceram. Soc.* **69** (1986) 564.
9. R. H. J. HANNINK, *J. Mater. Sci.* **13** (1978) 2487.
10. J. P. HIRTH and J. LOTHE, "Theory of dislocations" (Wiley, 1982).
11. V. PEROVIC, G. R. PURDY and L. M. BROWN, *Scripta Metall.* **15** (1980) 217.
12. D. G. JENSEN, R. H. J. HANNINK and B. C. MUDDLE, in "Proceedings of the 3rd IUMRS–ICAM Conference", Symposium J. Japan (1993).

Received 31 August 1994
and accepted 5 April 1995